Acta Mechanica 49, 57—79 (1983)

ACTA MECHANICA

Rigid Granular Plasticity Model and Bifurcation in the Triaxial Test

By

I. Vardoulakis, Minneapolis, Minnesota

With 10 Figures

(*Received October 8, 1982*)

Summary

Diffuse and localized bifurcation modes in axisymmetric, rectilinear deformations on rigid-granular dilatant material are analyzed. Rigid-granular behavior is described by a Mohr-Coulomb, single-hardening, rigid-plastic model with non-associated flow rule. Diffuse bulging in the compression test and diffuse necking in the extension test are always possible in the vicinity of the plastic limiting state. Localizations in the compression test occur in the softening regime, and in the extension test they occur in the hardening regime of the considered stress ratio-strain curve.

Introduction

In recent publications Needleman [1] and Vardoulakis [2] showed that the mathematical structure of the bifurcation problems related to plane-rectilinear deformations on pressure-sensitive and dilatant materials is the same as the one for pressure-insensitive and incomporessible materials, presented earlier by Hill and Hutchinson [3] and Young [4]. Concerning axisymmetric motions of extension, Cheng et al. [5] and Hutchinson and Miles [6] formulated the bifurcation problem for cylindrical specimens of elastic-plastic and incompressible material. In recent years the author published a paper [7] concerning the bifurcation phenomena in the triaxial test on dry sand samples, i.e., pressure-sensitive, dilatant material. The resultant differential equation, governing diffuse bifurcation modes, was different from the one holding for elastic-plastic and incompressible material. This anomaly in the mathematical structure triggered a reconsideration of the problem. It was concluded that the difference in the governing differential equation arose from unnecessary approximations, introduced by the author, in the linearization procedure of the incrementally non-linear constitutive equations, (see second chapter). In this paper the correct linearization is used, and the solution of the problem regains its simplicity.

Based on the constitutive model presented by Stören and Rice [8], the author has shown [9] that a small-strain deformation theory of plasticity for rigid granular and dilatant material can produce the total-strain formulation of the deviatoric part of the yield-vertex model studied by Rudnicki and Rice

0001-5970/83/0049/0057/$04.60

[10]. In a recent publication [11] the author has presented a modification of the rigid-granular model by incorporating in it a more general deviatoric flow rule. This modification allows for the description of anisotropic behavior for small perturbations of the strain rate in the vicinity of triaxial compression or extension; this anisotropy is expressed by two different incipient shear moduli μ and $\mathring{\mu}$ in (r, z) — and (r, θ) — axes, respectively. In the present paper the rigid granular constitutive model, presented in Ref. [11], is used. The main characteristics of this model are 1) a Mohr-Coulomb yield condition, 2) a non-associated volumetric and deviatoric flow rule, and 3) the assumption that dilatancy is an internal constraint. Consistent with (3) is the assumption that the mean pressure increment is kinematically indeterminante.

The bifurcation problem is formulated semi-inversely in terms of a perturbation solution. At the moment of bifurcation, nearly proportional loading in the sense of Shanley [12] is assumed; i.e., this perturbation technique allows a linearlization of the constitutive equations, which holds for small deviations from the "straight ahead" continuation of the preceding loading history (see Refs. [2], [7], [9]).

In the next chapter the bifurcation problem is formulated, and the field equations and compatibility conditions are given. Subsequently, the constitutive equations for the rigid-granular, dilatant material are presented and discussed. The field equations for the perturbation solution are then expressed in terms of an appropriate stream function Ψ, and the governing differential equation or Ψ is derived. Discontinuous modes analysis and classification of regimes are then presented. Diffuse bifurcation modes of the triaxial with mixed boundary conditions are analyzed, and the corresponding eigenvalue equations for the physically significant cases are formulated. The eigenvalue equations are then numerically solved for special values of the material properties, which are characteristic for medium-grained sand. The numerical results are finally discussed in the light of the experimental evidence.

Kinematic and Static Considerations

Let a homogeneous, cylindrical, dry-sand specimen in an undistorted initial configuration $\varkappa_1$ be subjected to a smooth, quasi-static, axisymmetric motion of extension. Call the resultant configuration of the speciment $\varkappa$. Let $\varkappa$ be the reference configuration, R the radius, and H the height of the sand specimen in $\varkappa$ (Fig. 1a). A single, fixed, cylindrical coordinate system is introduced, with its z-axis along the axis of the specimen.

Let

$$x_1 = r, \qquad x_2 = \theta, \qquad x_3 = z \tag{1}$$

be the cylindrical coordinates of a particle X in $\varkappa$. Let v_i be the velocity field in $\varkappa$. The bifurcation mode is assumed to be a linear combination of a homogeneous axisymmetric motion of extension v_i^0 and an inhomogeneous perturbation solution Δv_i [2], [7], [9]:

$$v_i = v_i^0 + \Delta v_i \qquad (\|\Delta v_i\| \ll \|v_i^0\|). \tag{2}$$

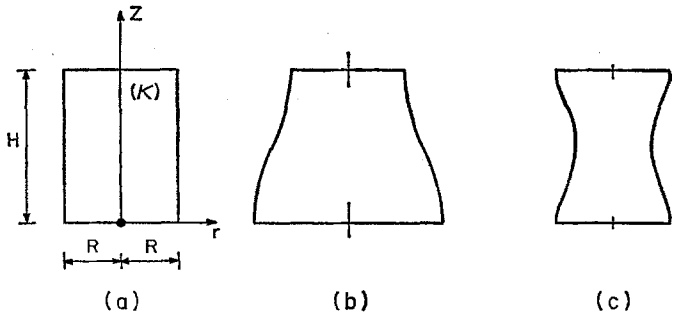

Fig. 1. *a* Geometric properties of the sample, *b* Bulging mode for compression, *c* Necking mode for extension

This restriction is necessary for linearizing the incrementally non-linear constitutive equations discussed here [see (34) and (37)].

v_i^0 is called the trivial mode and has the following form:

$$v_r^0 = \dot{q}_r \frac{r}{R}; \qquad v_\theta^0 = 0; \qquad v_z^0 = \dot{q}_z \frac{z}{H}, \tag{3}$$

where $\dot{q}_r$ and $\dot{q}_z$ are constants. The non-trivial mode Δv_i is a small perturbation with respect to the trivial mode v_i^0. Let

$$v_r = v_r(r, z), \qquad v_\theta = 0, \qquad v_z = v_z(r, z) \tag{4}$$

be the physical components of the considered velocity field (2). The phyiscal components $\dot{\varepsilon}_{ij}$ of the strain-rate tensor and the physical components $\dot{\omega}_{ij}$ of the spin tensor are:

$$\dot{\varepsilon}_{rr} = \frac{\partial v_r}{\partial r}, \qquad \dot{\varepsilon}_{zz} = \frac{\partial v_z}{\partial z}, \qquad \dot{\varepsilon}_{rz} = \frac{1}{2}\left(\frac{\partial v_r}{\partial z} + \frac{\partial v_z}{\partial r}\right) \tag{5}$$

$$\dot{\omega}_{zr} = -\dot{\omega}_{rz} = \dot{\omega} = \frac{1}{2}\left(\frac{\partial v_z}{\partial r} - \frac{\partial v_r}{\partial z}\right).$$

All other components not listed above are zero. The deviator of the strain rate tensor is denoted by $\dot{e}_{ij}$.

The physical components of the Cauchy stress in $\varkappa$ are denoted by σ_{ij}:

$$(\sigma_{ij}) = \begin{bmatrix} \sigma_r & 0 & 0 \\ 0 & \sigma_\theta & 0 \\ 0 & 0 & \sigma_z \end{bmatrix} \tag{6}$$

where

$$\sigma_z < \sigma_\theta = \sigma_r < 0 \qquad \textit{for compression} \tag{7}$$

and

$$\sigma_r = \sigma_\theta < \sigma_z < 0 \qquad \textit{for extension.} \tag{8}$$

Note that throughout this paper *compression is taken as negative.*

Constitutive equations are formulated in terms of a stress rate which is invariant in respect to rotation [13]. Let $\dot{\sigma}_{ij}$ denote the rate of the Cauchy stress tensor and $\overset{\nabla}{\sigma}_{ij}$ denote the Jaumann derivative of the Cauchy stress tensor:

$$\overset{\nabla}{\sigma}_{ij} = \dot{\sigma}_{ij} - \dot{\omega}_{ik}\sigma_{kj} + \sigma_{ik}\dot{\omega}_{kj}. \tag{9}$$

Continued equilibrium is expressed in terms of the rate $\dot{\Sigma}_i^{\,k}$ of the 1. Piola-Kirchhoff stress tensor [14]:

$$\dot{\Sigma}_i^{\,k}|_k = 0, \tag{10}$$

where $(\cdot)|_i$ denotes covariant differentiation. The physical components $\dot{\Sigma}_{ij}$ of the rate of the 1. Piola-Kirchhoff stress tensor are related to the co-rotational stress rate by the following Eqs. [14], [15]:

$$\dot{\Sigma}_{ij}' = \overset{\nabla}{\sigma}_{ij} + \dot{\omega}_{ik}\sigma_{kj} - \sigma_{ik}\dot{\varepsilon}_{kj} + \sigma_{ij}\dot{\varepsilon}_{kk}. \tag{11}$$

For the considered state of prestress (6), (10) and (11) yield [7]:

$$\begin{aligned} &\frac{\partial \overset{\nabla}{\sigma}_{rr}}{\partial r} + \frac{\partial \overset{\nabla}{\sigma}_{rz}}{\partial z} + \frac{1}{r}\left(\overset{\nabla}{\sigma}_{rr} - \overset{\nabla}{\sigma}_{\theta\theta}\right) + 2t\frac{\partial \dot{\omega}}{\partial z} = 0 \\ &\frac{\partial \overset{\nabla}{\sigma}_{rz}}{\partial r} + \frac{\partial \overset{\nabla}{\sigma}_{zz}}{\partial z} + \frac{1}{r}\overset{\nabla}{\sigma}_{rz} + 2t\left(\frac{\partial \dot{\omega}}{\partial r} + \frac{\dot{\omega}}{r}\right) = 0 \end{aligned} \tag{12}$$

where

$$t = (\sigma_r - \sigma_z)/2 \tag{13}$$

is positive for compression and negative for extension.

Let S be a stationary discontinuity surface of the velocity gradient, and let n_i be the unit normal vector on S in x. Denoting the physical components of the velocity gradient by $v_{\langle i|j\rangle}$, the geometrical compatibility conditions across S read [13], [15]:

$$[v_{\langle i|j\rangle}] = g_i n_j, \tag{14}$$

where $[\cdot]$ denotes the jump of a quantity across S. Continued equilibrium across S is expressed by the following statical compatibility conditions [13], [15]:

$$[\dot{\Sigma}_{ij}]\, n_j = 0. \tag{15}$$

The observed discontinuous deformation modes in the triaxial test are: 1) rigid cones at the ends of the specimen and shear bands in the compression test, and 2) localized necking in the extension test. It is assumed that all these formations are bounded by weak, stationary, discontinuity surfaces in the displacement gradient. Axially symmetric discontinuities are discribed by the conditions [9]:

$$g_\theta = n_\theta = 0. \tag{16}$$

The above conditions describe also a set of shear bands, equally inclined against the z-axis.

For the considered state of prestress (6), the statical compatibility conditions (15) with (11) and (16) yield [9]:

$$\begin{aligned} \left[\overset{\nabla}{\sigma}_{rr}\right] n_r + \left(\left[\overset{\nabla}{\sigma}_{rz}\right] + 2t[\dot{\omega}]\right) n_z = 0 \\ \left(\left[\overset{\nabla}{\sigma}_{zr}\right] + 2t[\dot{\omega}]\right) n_r + \left[\overset{\nabla}{\sigma}_{zz}\right] n_z = 0. \end{aligned} \tag{17}$$

Constitutive Equations

For the considered state of prestress (6), the Mohr-Coulomb yield condition for a material full of friction can be expressed in terms of the mobilized friction angle ϕ_m, defined by:

$$\sin \phi_m = \left| \frac{\sigma_r - \sigma_z}{\sigma_r + \sigma_z} \right|. \tag{18}$$

Let

$$\tau = \left(\frac{3}{2} s_{lk} s_{kl} \right)^{1/2}; \qquad p = \sigma_{kk}/3 \tag{19.1,2}$$

where s_{ij} is the deviator of the Cauchy stress tensor σ_{ij}. The friction law can also be expressed in terms of the stress obliquity ϕ_σ, defined by

$$\sin \phi_\sigma = \frac{\tau}{3\,|p|}. \tag{20}$$

For the considered state of prestress (6)

$$\sin \phi_\sigma = \frac{2 \sin \phi_m}{3 \mp \sin \phi_m}; \tag{21}$$

when two signs appear, the upper sign applies for the triaxial compression (7) and the lower sign applies for the triaxial extension (8), unless otherwise stated.

It is assumed that for continuous loading, ϕ_m obeys a strain-hardening rule

$$\operatorname{sind} \phi_m = F(g), \tag{22}$$

where $F(\cdot)$ is a hardening function and g a finite Eulerian measure of the shearing intensity of the deformation measured from the initial configuration $\varkappa_1$. g is defined here as logarithmic strain:

$$g = \left(\frac{3}{2} e_{ij} e_{ji} \right)^{1/2} = |\varepsilon_r - \varepsilon_z| = \left| \ln \left(\frac{R}{R_1} \right) - \ln \left(\frac{H}{H_1} \right) \right|, \tag{23}$$

where R_1 and H_1 are the radius and the height, respectively, of the specimen in the initial configuration $\varkappa_1$.

Let h_m be the slope of the stress ratio-strain curve (22), given by

$$h_m = \frac{d \sin \phi_m}{dg}. \tag{24}$$

Using (21) and (24), we introduce the following tangential hardening modulus:

$$h_t = \frac{d \sin \phi_\sigma}{dg} = \frac{6 h_m}{(3 \mp \sin \phi_m)^2}. \tag{25}$$

With the notation given in (19), from (20) and (25) it follows that:

$$\dot{\tau} + 3\dot{p} \sin \phi_\sigma + 3 p h_t \dot{g} = 0. \tag{26}$$

For the considered motions of extension $\varkappa_1 \to \varkappa$, $\dot{g}$ coincides with the shearing intensity $\dot{\gamma}^0$ of the strain-rate tensor. With

$$\dot{\gamma} = \left(\frac{3}{2} \dot{e}_{ij} \dot{e}_{ji} \right)^{1/2} \tag{27}$$

and the perturbation solution (2), $\dot{\gamma}$ can be linearized as follows:

$$\dot{\gamma} = \dot{\gamma}^0 + \left(\frac{\partial \dot{\gamma}}{\partial \dot{e}_{kl}} \right)_0 \Delta \dot{e}_{kl} = |\dot{\varepsilon}^0_{rr} - \dot{\varepsilon}^0_{zz}| \mp \frac{3}{2} \Delta \dot{e}_{zz}. \tag{28}$$

Similarly, from (19.1) one can deduce

$$\dot{\tau} = \left| \overset{\nabla}{\sigma}{}^0_{rr} - \overset{\nabla}{\sigma}{}^0_{zz} \right| \mp \frac{3}{2} \Delta \overset{\nabla}{\sigma}_{zz}. \tag{29}$$

In our previous analyses [7], [9], we introduced the approximations $\dot{e}_{zz} \simeq 2 \cdot (\dot{\varepsilon}_{zz} - \dot{\varepsilon}_{rr})/3$ and $\overset{\nabla}{s}_{zz} \simeq 2 \left(\overset{\nabla}{\sigma}_{zz} - \overset{\nabla}{\sigma}_{rr} \right)/3$. As mentioned in the introduction, these approximations, yielded finally to a more complex mathematical model, since the governing differential equation did not become a well-documented one.

Introducing (28) and (29) into (26), we obtain the following condition for continued yielding:

$$\Delta \overset{\nabla}{\sigma}_{zz} = (1 \pm 2 \sin \phi_\sigma) \Delta \overset{\nabla}{p} + 2 \mu_t \Delta \dot{e}_{zz}, \tag{30}$$

where the tangent modulus μ_t is given by

$$\mu_t = \frac{3}{2} |p| h_t. \tag{31}$$

In order to describe axisymmetric bifurcation modes, we introduce two further incipient shear moduli μ and $\mathring{\mu}$, describing shear in (r, z)-axes and (r, θ)-axes respectively. The constitutive equations for the considered perturbations take

the following form:

$$\begin{aligned}
\overset{\nabla}{\sigma}_{rr} &= (1 \mp \sin\phi_\sigma)\overset{\nabla}{p} + \mathring{\mu}(\dot{\varepsilon}_{rr} - \dot{\varepsilon}_{\theta\theta}) - \mu_t \dot{e}_{zz} \\
\overset{\nabla}{\sigma}_{zz} &= (1 \pm 2\sin\phi_\sigma)\overset{\nabla}{p} + 2\mu_t \dot{e}_{zz} \\
\overset{\nabla}{\sigma}_{rr} &- \overset{\nabla}{\sigma}_{\theta\theta} = 2\mathring{\mu}(\dot{\varepsilon}_{rr} - \dot{\varepsilon}_{\theta\theta}) \\
\overset{\nabla}{\sigma}_{rz} &= 2\mu\dot{\varepsilon}_{rz}.
\end{aligned} \tag{32}$$

The small-strain deformation theory of plasticity, derived in Ref. [9], reduces to (32) if the state of prestress (7) or (8) is assumed. In this case the incipient shear moduli μ and $\mathring{\mu}$ are equal (isotropy) and proportional to the governing mean pressure, and also proportional to the secant modulus h_s of the assumed $(\sin\phi_\sigma, g)$-curve:

$$\mu = \mathring{\mu} = \frac{3}{2}|p|\, h_s; \qquad h_s = \frac{\sin\phi_g}{g}. \tag{33}$$

This isotropy property is a direct consequence of the von Mises deviatoric flow rule, inherent in the constitutive equation of this type. As has been found experimentally by Goldscheider [16], the deviatoric flow rule for dry sand deviates essentially from that of von Mises. Following the investigations by Kolymbas [17] on constitutive equations of the rate type for soils, the author has recently presented a modification of the rigid granular model, in which the correction to the von Mises deviatoric flow rule is incorporated [11]. The deviatoric stress rates are then given by the following constitutive equations:

$$\begin{aligned}
\overset{\nabla}{s}_{ij} = &\left\{\frac{\overset{\nabla}{p}}{p} + 3p(h_1 - h)\frac{s_{kl}\dot{e}_{lk}}{s_{mn}s_{nm}}\right\} s_{ij} \\
&- 3ph_1\left\{\dot{e}_{ij} - \frac{\chi}{\left(\frac{2}{3}\dot{e}_{mn}\dot{e}_{nm}\right)^{1/2}}\left(\dot{e}_{ik}\dot{e}_{kj} - \frac{1}{3}\dot{e}_{kl}\dot{e}_{lk}\delta_{ij}\right)\right\},
\end{aligned} \tag{34}$$

where the hardening parameters h and h_1 are functions of g.

The constitutive Eqs. (34) can be evaluated for the state of prestress (7) or (8) and linearized in the sense of (28) and (29) for the considered perturbations. The linearized equations yield to (32) with the following expressions for the incipient shear moduli:

$$\begin{aligned}
\mu_t &= \frac{3}{2}|p|\, h_t; \qquad h_t = h \pm \chi h_1/2 \\
\mu &= \frac{3}{2}|p|\, h_1(1 \pm \chi/2); \qquad \mathring{\mu} = \frac{3}{2}|p|\, h_1(1 \mp \chi).
\end{aligned} \tag{35}$$

From (35) it follows that the shear-modulus ratio $\mathring{\mu}/\mu$ is fully determined from the deviatoric flow-rule parameter χ:

$$\frac{\mathring{\mu}}{\mu} = \frac{1 \mp \chi}{1 \pm \chi/2}. \tag{36}$$

For $\chi = 0$ this model reduces to the isotropic one corresponding to (33). The experimental results from Goldscheider are approximated with $\chi \simeq 0.55$ [11], [17]. As can be seen from (32) and (35), the hardening function h_1 can be measured in the strain-controlled, 'true-triaxial' test (cf. [16]): at a state $\varkappa$, reached by an axisymmetric motion of extension, an infinitesimal motion of extension is superimposed with, e.g., $\Delta\varepsilon_{zz} = 0$ and $\Delta\varepsilon_{rr} \neq \Delta\varepsilon_{\theta\theta}$. Experimental results of this type are not available in the literature. This means that in our following evaluations, h_1 will be an open parameter. Especially here h_1 is understood as a secant-type modulus, i.e., $h_1 > 0$ [18]. However, in a recent paper by Mehrabadi and Cowin [19] comparisons of rigid-granular model with the sliding-plasticity models for plane problems yielded to the suggestion of h_1 being negative. The author has shown in Ref. [11] that the present constitutive model (34) is not compatible with the assumption of a negative h_1. This is a direct consequence of the characteristic regimes of the localization condition for plane strain (see also Fig. 4).

The rigid-granular behavior is not completely described by the constitutive Eqs. (34). In addition to (34), the following assumptions must be made [7], [9]: 1) the mean pressure rate $\overset{\nabla}{p}$ in (34) is kinematically indeterminate, and 2) the strainrate obeys a geometric constraint of the form:

$$\dot{\varepsilon}_{kk} = \beta \left(\frac{3}{2} \dot{e}_{mn} \dot{e}_{nm} \right)^{1/2}, \tag{37}$$

where the dilatancy parameter β is a function of g.

For the considered perturbation solution (2), the dilatancy constraint (37) can be linearized using (28) and (29) as follows:

$$\dot{\varepsilon}_{zz} = -\frac{1}{\delta^2} (\dot{\varepsilon}_{rr} + \dot{\varepsilon}_{\theta\theta}), \tag{38}$$

where

$$\delta^2 = \frac{1 \pm \beta}{1 \mp \beta/2}. \tag{39}$$

The Volumetric Flow-Rule

The volumetric flow-rule is expressed by means of a *non-associated* flow-rule in which Rowe's [20] stress-dilatancy principle is incorporated. The stress-dilatancy principle for the triaxial test reads:

$$\frac{\sigma_z \dot{\varepsilon}_z}{2\sigma_r \dot{\varepsilon}_r} = -\lambda_c^2, \tag{40}$$

where λ_c^2 is a material constant. Let λ^2 denote the principal stress ratio in $\varkappa$:

$$\lambda^2 = \frac{\sigma_z}{\sigma_r} = \frac{1 \pm 2 \sin \phi_\sigma}{1 \mp \sin \phi_\sigma} = \tan^2 (45° \pm \phi_m/2). \tag{41}$$

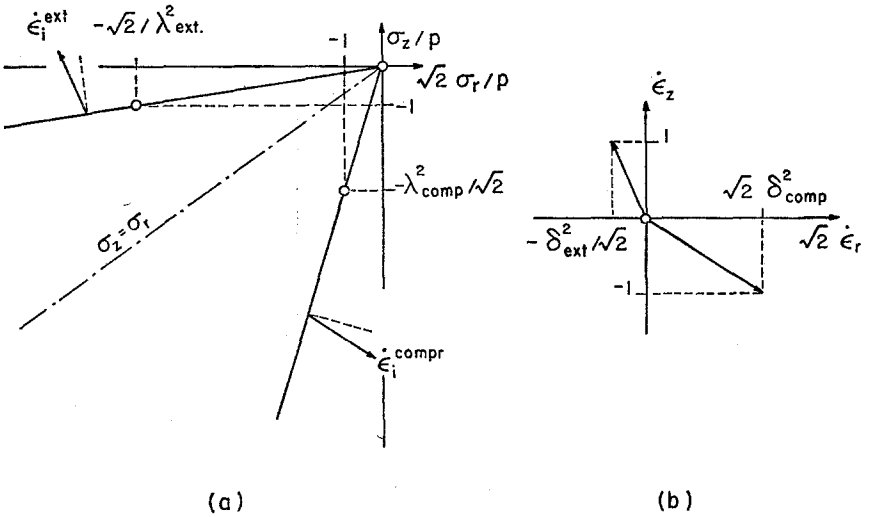

Fig. 2. Yield condition and non-associated flow rule ($\phi_p = 40°$; $\phi_c = 30°$)

From (40) and (41) it follows that λ_c^2 denotes the stress ratio in a state of isochoric deformation. From (38) to (41), a simple formula for δ follows [2], [18]:

$$\delta = \lambda/\lambda_c. \tag{42}$$

Fig. 2 illustrates the assumed linear Mohr-Coulomb yield condition and the corresponding non-associated volumetric flow-rule.

Normality and Experimental Evidence

Fig. 3 shows the experimental results from a triaxial compression test, performed by Hettler [21] on Karlsruhe sand that was dry, medium-grained, and dense. The dimensions of the specimen were chosen in such a fashion that disturbances in the homogeneity of the deformation due to bulging or due to imperfections in the specimen's height should not be influential.

From Fig. 3 it follows that λ_c^2, computed using (42) and the experimental results at the 'peak' state of maximum stress-ratio and dilatancy, coincides with the value of the stress-ratio at the state of initial isochoric deformation. By introducing the mobilized friction angle ϕ_c at the state of initial isochoric deformation, λ_c is given by

$$\lambda_c^2 = \left(\frac{\sigma_z}{\sigma_r}\right)_{\dot{\varepsilon}_{kk}=0} = \tan^2(45° \pm \phi_c/2). \tag{43}$$

Normality, expressed by the requirement $\sigma_{ij}\dot{\varepsilon}_{ij} = 0$, would yield the condition $\delta = \lambda$, or, according to (42) and (43), $\lambda_c = 1$ and $\phi_c = 0$, respectively. Fig. 3b shows a well-established experimental finding which falsifies normality. Starting from an isotropic state $\varkappa_1$, a small, superimposed deviatoric stress will always produce an initial contraction. This can be explained microscopically by the change in fabric induced by the superimposed deviator.

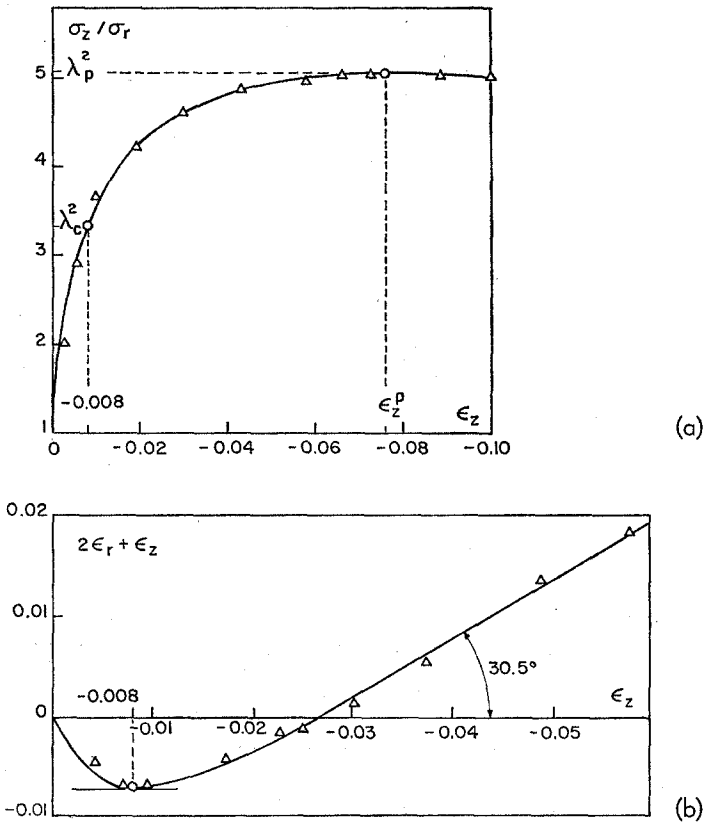

Fig. 3. Experimental results by Hettler [21]
($n_1 = 0.366$; $\sigma_c = 400$ kN/m²; $R/H = 39.5$ cm/27.5 cm)
a Stress ratio-axial strain curve, *b* Volumetric strain-axial strain curve

Field Equations

Assuming that the trivial mode (3) satisfies the dilatancy constraint (38) and introducing a stream function $\Psi(r, z)$ such that

$$\Delta v_r = \frac{\partial \Psi}{\partial z} \qquad \text{and} \qquad \Delta v_z = -\frac{1}{\delta^2}\frac{1}{r}\frac{\partial (r\Psi)}{\partial r}, \tag{44}$$

it follows that the non-trival mode Δv_i also satisfies the dilatancy constraint. Introducing (44) into (5) yields:

$$\Delta \dot{\varepsilon}_{rr} = \frac{\partial^2 \Psi}{\partial r\, \partial z}; \qquad \Delta \dot{\varepsilon}_{\theta\theta} = \frac{1}{r}\frac{\partial \Psi}{\partial z}; \qquad \Delta \dot{\varepsilon}_{zz} = -\frac{1}{\delta^2}\frac{\partial}{\partial z}\left\{\frac{1}{r}\frac{\partial (r\Psi)}{\partial r}\right\}$$
$$2\Delta \dot{\varepsilon}_{rz} = -\frac{1}{\delta^2} L_r(\Psi) + \frac{\partial^2 \Psi}{\partial z^2}; \qquad 2\Delta \dot{\omega} = -\frac{1}{\delta^2} L_r(\Psi) - \frac{\partial^2 \Psi}{\partial z^2}, \tag{45}$$

where the operator L_r is defined as follows [5], [6]:

$$L_r = \frac{\partial^2}{\partial r^2} + \frac{1}{r}\frac{\partial}{\partial r} - \frac{1}{r^2}. \tag{46}$$

From (45) and (32) the stress-rate increments can be computed:

$$\begin{aligned}
\overset{\nabla}{\Delta\sigma}_{rr} &= (1 \mp \sin\phi_\sigma)\,\overset{\nabla}{\Delta p} + \mathring{\mu}\,\frac{\partial}{\partial z}\left\{r\,\frac{\partial}{\partial r}\left(\frac{\Psi}{r}\right)\right\} + \frac{2+\delta^2}{3\delta^2}\,\mu_t\,\frac{\partial}{\partial z}\left\{\frac{1}{r}\,\frac{\partial}{\partial r}\,(r\Psi)\right\}\\
\overset{\nabla}{\Delta\sigma}_{zz} &= (1 \pm 2\sin\phi_\sigma)\,\overset{\nabla}{\Delta p} - 2\,\frac{2+\delta^2}{3\delta^2}\,\mu_t\,\frac{\partial}{\partial z}\left\{\frac{1}{r}\,\frac{\partial}{\partial r}\,(r\Psi)\right\}\\
\overset{\nabla}{\Delta\sigma}_{rr} - \overset{\nabla}{\Delta\sigma}_{\theta\theta} &= 2\mathring{\mu}\,\frac{\partial}{\partial z}\left\{r\,\frac{\partial}{\partial r}\left(\frac{\Psi}{r}\right)\right\}\\
\overset{\nabla}{\Delta\sigma}_{rz} &= \mu\left\{-\frac{1}{\delta^2}\,L_r(\Psi) + \frac{\partial^2\Psi}{\partial z^2}\right\}.
\end{aligned} \tag{47}$$

Taking into account that the trivial mode (3) produces a constant strain field, from the field Eqs. (12) and the above representations (47) it follows that

$$\begin{aligned}
-(1 \mp \sin\phi_\sigma)\,\frac{\partial \overset{\nabla}{\Delta p}}{\partial r} &= \frac{\partial}{\partial z}\left\{\left(\mathring{\mu} + \frac{2+\delta^2}{3\delta^2}\,\mu_t - \frac{1}{\delta^2}\,(\mu + t)\right) L_r(\Psi) + (\mu - t)\,\frac{\partial^2\Psi}{\partial z^2}\right\}\\
-(1 \pm 2\sin\phi_\sigma)\,\frac{\partial \overset{\nabla}{\Delta p}}{\partial z} &= -(\mu + t)\,\frac{1}{\delta^2}\,\frac{1}{r}\,\frac{\partial}{\partial r}\left(rL_r(\Psi)\right)\\
&\quad + \left(\mu - t - 2\,\frac{2+\delta^2}{3\delta^2}\,\mu_t\right)\frac{\partial^2}{\partial z^2}\left(\frac{1}{r}\,\frac{\partial}{\partial r}\,(r\Psi)\right).
\end{aligned} \tag{48}$$

Differentiation and combination of the above field equations to eliminate $\overset{\nabla}{\Delta p}$, which is kinematically indeterminate, yield one equation for the stream function Ψ:

$$L_r^2(\Psi) + A\,\frac{\partial^2}{\partial z^2}\,L_r(\Psi) + B\,\frac{\partial^4\Psi}{\partial z^4} = 0, \tag{49}$$

where

$$\begin{aligned}
A &= \left(a_0\frac{t}{\mu} + a_1\right)\Big/\left(1 + \frac{t}{\mu}\right)\\
a_0 &= -\lambda^2 + \delta^2 \pm a h_t; \qquad a = (2+\delta^2)\,(2+\lambda^2)/(3\sin\phi_\sigma)\\
a_1 &= -\lambda^2 - \delta^2 + \lambda^2\delta^2\,\frac{\mathring{\mu}}{\mu}\\
B &= \lambda^2\delta^2\left(1 - \frac{t}{\mu}\right)\Big/\left(1 + \frac{t}{\mu}\right).
\end{aligned} \tag{50}$$

Eq. (49) is a 4th-order, partial differential equation of the mixed type. The above derivation illustrates that the particular linearization described here yields a governing equation having the same form as that obtained by Cheng et al. [5] and in Hutchinson and Miles [6] in the analyses of axisymmetric bifurcation

modes in elastic-plastic incompressible cylinders. The same conclusion is drawn from the corresponding bifurcation analyses of plane-strain rectilinear deformations [1], [2], [3], [4].

Discontinuous Modes and Classification of Regimes

The analysis of discontinuous bifurcation modes in the triaxial test on pressure-sensitive material appeared first in a paper by Rudnicki and Rice [10] and later in Vardoulakis [9]. The compatibility conditions for the stress and strain field across a given weak, stationary, discontinuity surface S in x are expressed by (14) and (17). By introducing the geometrical compatibility conditions (14) and the symmetry condition (16) into the dilatancy constraint (38), the following kinematical constraint is derived:

$$g_r n_r = -\delta^2 g_z n_z. \tag{51}$$

The statical compatibility conditions (17) are evaluated using the constitutive Eqs. (32) and the jump conditions (14), (16), and (51). Elimination of the jump $[\Delta \overset{\nabla}{p}]$ from the statical compatibility conditions finally yields the following wells known form of the condition for discontinuous solutions:

$$n_r^4 + A n_r^2 n_z^2 + B n_z^4 = 0, \tag{52}$$

where A and B are given by (50). Eq. (52) is called the *characteristic equation.*

The type of the governing differential Eq. (49) depends on the type of the roots of the characteristic Eq. (52). Let

$$\Gamma = n_r/n_z; \qquad D_0 = A^2 - 4B. \tag{53}$$

The characteristic regimes of (52) are classified as follows:

EC (elliptic-complex): $B > 0; \quad D_0 < 0$

$$\begin{gathered} \Gamma_{1/2} = \pm c; \qquad \Gamma_{3/4} = \pm \bar{c}; \qquad c = M + iN; \qquad i = \sqrt{-1} \\ M = \left(\left(\sqrt{B} - A/2\right)/2\right)^{1/2}; \qquad N = \left(\left(\sqrt{B} + A/2\right)/2\right)^{1/2} \end{gathered} \tag{54}$$

EI (elliptic-imaginary): $A > 0 \quad (B > 0); \quad D_0 > 0$

$$\begin{gathered} \Gamma_{1/2} = \pm i c_1; \qquad \Gamma_{3/4} = \pm i c_2 \\ c_{1/2} = \left(\left(A \pm \sqrt{D_0}\right)/2\right)^{1/2} \end{gathered} \tag{55}$$

P (parabolic): $B < 0 \ (D_0 > 0)$

$$\begin{gathered} \Gamma_{1/2} = \pm c_1; \qquad \Gamma_{3/4} = \pm i c_2 \\ c_{1/2} = \left(\left(\sqrt{D_0} \mp A\right)/2\right)^{1/2}. \end{gathered} \tag{56}$$

H (hyperbolic): $A < 0; \quad B > 0; \quad D_0 > 0$

$$\begin{gathered} \Gamma_{1/2} = \pm c_1; \qquad \Gamma_{3/4} = \pm c_2 \\ c_{1/2} = \left(\left(-A \pm \sqrt{D_0}\right)/2\right)^{1/2}. \end{gathered} \tag{57}$$

The boundaries between the characteristic regimes are classified as follows:

EC/EI: $A > 0$; $\quad D_0 = 0$

$$\Gamma_{1/2,3/4} = \pm ic; \qquad c = (A/2)^{1/2} \tag{58}$$

EC/H: $A < 0$; $\quad D_0 = 0$

$$\Gamma_{1/2,3/4} = \pm c; \qquad c = (-A/2)^{1/2} \tag{59}$$

E/P: $A > 0$; $\quad B = 0$

$$\Gamma_{1/2} = 0; \qquad \Gamma_{3/4} = \pm i\sqrt{A} \tag{60}$$

H/P $\subset$ *H:* $A < 0$; $\quad B = 0$

$$\Gamma_{1/2} = 0; \qquad \Gamma_{3/4} = \pm\sqrt{-A}. \tag{61}$$

Discussion of the Characteristic Equation

The discriminant D_0, given by $(53)_2$, can be looked upon as a rational function of t/μ:

$$D_0 = \left\{A_0 \left(\frac{t}{\mu}\right)^2 + 2A_1 \frac{t}{\mu} + A_2\right\} \Big/ \left(1 + \frac{t}{\mu}\right), \tag{62}$$

$$A_0 = a_0{}^2 + 4\lambda^2\delta^2; \qquad A_1 = a_0 a_1; \qquad A_2 = a_1{}^2 - 4\lambda^2\delta^2, \tag{63}$$

where a_0 and a_1 are defined by (50). Let ξ_1, ξ_2 be the roots of the equation $D_0\left(\frac{t}{\mu}\right) = 0$, thereby characterizing the *EC/EI*- and *EC/H*-boundaries:

$$\xi_{1/2} = \left(-A_1 \pm \sqrt{D_1}\right)/A_0, \tag{64}$$

where

$$D_1 = A_1{}^2 - A_0 A_2. \tag{65}$$

The characteristic regimes of (52) are represented graphically in a $\left(\frac{t}{\mu}\text{ vs. } h_t\right)$-state diagram. Fig. 4 shows the characteristic regimes in the vicinity of the 'peak' of the stress ratio-strain curve ($h_t = 0$) and for a triaxial extension test. The assumed values for the peak friction angle ϕ_p and the dilatancy parameter β are taken from Reads and Green [22], Fig. 6 and Fig. 10, respectively; i.e., $\phi_p = 46°$, $\beta = 0.273$ ($\phi_c = 36.4°$). With $\chi = 0$ ($\mathring{\mu} = \mu$) Fig. 4 is characteristic for a dense sand obeying the von Mises deviatoric flow rule. On this diagram one recognizes two characteristic points R_1 and R_2 with the properties:

$$\frac{t}{\mu} = \xi^R; \qquad \xi^R = -A_1/A_0 \tag{66.1}$$

$$h_t = h_{1/2}^R = \left((\pm)\,(\lambda^2 - \delta^2) \pm \sqrt{D_2}\right)/a \tag{66.2}$$

$$D_2 = \lambda^4\delta^4 \left(\frac{\mathring{\mu}}{\mu} - M_1\right)\left(\frac{\mathring{\mu}}{\mu} - M_2\right) \tag{66.3}$$

$$M_{1/2} = \left(\frac{\lambda \pm \delta}{\lambda\delta}\right)^2. \tag{66.4}$$

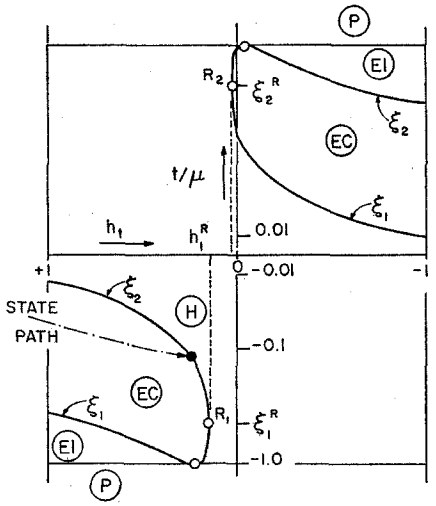

Fig. 4. Characteristic regime in the triaxial extension test and in the vicinity of the plastic limiting state ($\phi_p = 46°$; $\phi_c = 36.4°$; $\chi = 0$)

The alternative sign in parentheses in (66.2) holds for compression or extension, respectively. From (66.3) it follows that for $0 < \mathring{\mu}/\mu < M_1$ or $M_2 < \mathring{\mu}/\mu$, the characteristic diagram will show a 'closed' E-regime. In this case localization is inevitable since the actual state path will always intersect the EC/H-boundary. Fig. 4 shows that localized necking in the triaxial extension test on the considered sand will always occur in the hardening regime of the corresponding stress ratio-strain curve, i.e., for $h_t > h_1{}^R > 0$. From (66.2) it follows that this porperty is a direct consequence of the assumed non-associated volumetric flow rule ($\lambda < \delta$). These theoretical results are in accordance with the corresponding experimental findings by Reads and Green [22], who on p. 564 state that "... necking in an extension test sample increases rapidly post-failure, when deformations become concentrated in a small portion of the sample ..." From the corresponding, stress ratio-strain curves, which show a sharp peak (Fig. 15 in Ref. [22]), one recognizes the fact that localized necking is actually occurring in the hardening reigme as predicted. Fig. 4 shows, however, that localized necking is occurring very close to the plastic limit state ($h_t = 0$).

Orientation of Localizations

As already implied, localizations are assumed to occur as soon as the state path intersects the EC/H-boundary [3]. Let ψ be the inclination angle of the discontinuity plane bounding the localization, ψ being measured with respect to the r-axis:

$$\psi = \arctan\,(n_r/n_z). \tag{67}$$

For $D_0 = 0$ from (59) and (52) it follows that

$$\psi = \pm\arctan\,(B_i)^{1/4}, \tag{68}$$

where B_i is the value of B for $\frac{t}{\mu} = \xi_i$. A formula similar to (68) also holds for the plane-strain test [2], [18]. Fig. 5 shows the evaluation of (68) for the same material properties as the ones holding for the graph on Fig. 4 and for $h_t \geqq h_1^R$. For $\frac{t}{\mu} \ll 1$ from (68) the following approximative formula for the orientation angle $\psi \simeq \pm\psi_B$ can be deduced:

$$\psi_B = \arctan(\lambda\delta)^{1/2}. \tag{69}$$

Eq. (69) illustrates the fact that the orientation of the localization is governed by both the dilatancy and frictional characteristics of the material.

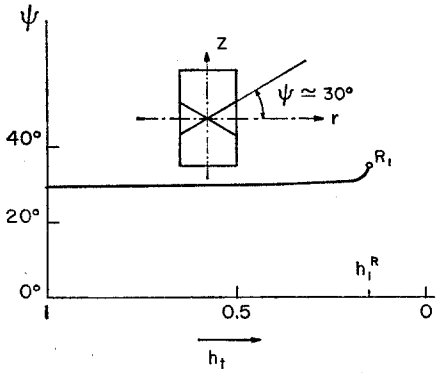

Fig. 5. Orientation of the localization in the triaxial extension test ($\phi_p = 46°$; $\phi_c = 36.4°$; $\chi = 0$)

Diffuse Bifurcation Modes

In this chapter we consider the physically significant, axisymmetric bifurcation modes in the triaxial test using cylindrical samples, mixed boundary conditions, and non-tilting top platen (Fig. 1b and 1c). On the edges $z = 0$ and $z = H$ lubrication prevents the build up of frictional constraints, so that at any state $\varkappa$ $\sigma_{rz} = 0$. On $z = H$ a uniform velocity $\dot{q}_z$ is prescribed, and the cylindrical surface is subjected to a hydrostatic confining pressure $\sigma_r = -\sigma_0$. As already mentioned, the trivial mode v_i^0 is a motion of extension, expressed by (3), which satisfies the boundary conditions. For the non-trivial mode Δv_i the following displacement field is tested:

$$\Delta v_r = u(\varrho)\cos\zeta, \qquad \Delta v_z = w(\varrho)\sin\zeta, \tag{70}$$

$$\varrho = r/R; \qquad \zeta = m\pi(z/H), \qquad m = 1, 2, \ldots \tag{71}$$

This field automatically satisfies homogeneous boundary conditions at the ends of the specimen:

$$\Delta v_z = 0; \qquad \Delta\overset{\nabla}{\sigma}_{rz} = 0 \qquad \text{for} \qquad z = 0 \qquad \text{and} \qquad z = H. \tag{72}$$

From (44) and (70) it follows that

$$\Psi = \frac{H}{m\pi}\, u(\varrho) \sin \zeta \tag{73}$$

and consequently

$$w = \frac{-1}{K\delta^2 \varrho}\, \frac{d(\varrho u)}{d\varrho}, \tag{74}$$

where

$$K = m\pi(R/H) \tag{75}$$

is the physical slenderness of the specimen. The following representation of the mean pressure increment $\overset{\nabla}{\Delta p}$ is consistent with the displacement field (70):

$$\overset{\nabla}{\Delta p} = p(\varrho) \cos \zeta. \tag{76}$$

For the considered stream function (73), (48) then yields the following expression for $p(\varrho)$:

$$\begin{aligned} p = \frac{-1}{1 \pm 2 \sin \phi_\sigma}\, \frac{1}{K^2 R \delta^2} \Big\{ & (\mu + t)\, \frac{1}{\varrho}\, \frac{d}{d\varrho} \left(\varrho L_\varrho(u)\right) \\ & + K^2 \left(-2\, \frac{2 + \delta^2}{3}\, \mu_t + \delta^2(\mu - t) \right) \frac{1}{\varrho}\, \frac{d}{d\varrho} (\varrho u) \Big\}. \end{aligned} \tag{77}$$

Substitution of Ψ from (73) into (49) yields finally the well-known governing differential equation for the considered bifurcation problem [5], [6]:

$$L_\varrho^2(u) - K^2 A L_\varrho(u) + K^4 B u = 0. \tag{78}$$

Due to the boundness condition of u at $\varrho = 0$, the solution of (78) has the form

$$u = C_1 u^{(1)} + C_2 u^{(2)} \qquad \text{and} \qquad u^{(i)} = J_1(K\Gamma_i \varrho), \tag{79}$$

where $J_1(\cdot)$ is the Bessel function of the first kind and first order and Γ_i satisfies the characteristic equation:

$$\Gamma_i^4 + A\Gamma_i^2 + B = 0. \tag{80}$$

Boundary Conditions

For the considered infinitesimal transition $\varkappa \to \varkappa'$ the boundary conditions for the unconfined sides of the specimen express the fact that a traction of constant intensity always acts normally on these boundaries. This condition then yields to the following requirements [7]:

$$\text{for} \qquad \varrho = 1: \quad \Delta\dot{\varepsilon}_{rz} = 0; \qquad \overset{\nabla}{\Delta\sigma}_{rr} = 0. \tag{81}$$

From (45), (47), (73), and (77), the above boundary conditions (81) yield

$$Q(u) = \left\{ \frac{1}{\varrho}\, \frac{d}{d\varrho} \left(\varrho L_\varrho(u)\right) - K^2 \left(q_1 \frac{du}{d\varrho} + q_2\, \frac{u}{\varrho} \right) \right\} \Big|_{\varrho=1} = 0, \tag{82}$$

$$P(u) = \{L_\varrho(u) + K^2\delta^2 u\}|_{\varrho=1} = 0, \tag{83}$$

where

$$q_i = \left(q_{i0}\frac{t}{\mu} + q_{i1}\right)\Big/\left(1 + \frac{t}{\mu}\right), \qquad i = 1, 2 \tag{84}$$

and

$$\begin{aligned} q_{10} &= q_{20} = \delta^2 \pm a h_t \\ q_{11} &= \lambda^2\delta^2\frac{\mathring{\mu}}{\mu} - \delta^2. \\ q_{21} &= -\lambda^2\delta^2\frac{\mathring{\mu}}{\mu} - \delta^2. \end{aligned} \tag{85}$$

By introducing u from (79) into (82) and (83), the bifurcation condition can be derived if we ask for non-trivial solutions for C_1 and C_2:

$$Q(u^{(1)})\,P(u^{(2)}) - Q(u^{(2)})\,P(u^{(1)}) = 0. \tag{86}$$

Eigenvalue Equations in the Elliptic Regime

Since soil specimens in triaxial testing always show localized failure patterns, it is meaningful to discuss only the diffuse bifurcation modes occurring prior to localization. Assuming that localization takes place on the *EC*/*H*-boundary, we will discuss here only the diffuse modes in the elliptic regime.

EC-Regime

The solution (79) in *EC* has the form

$$u = CJ_1(Kc_Q) + \bar{C}J_1(K\bar{c}_Q), \tag{87}$$

where c is given by (54). For this representation of u, the bifurcation condition (86) can be written as follows [6]:

$$\operatorname{Im}\left\{(\delta^2 - \bar{c}^2)\,J_1(K\bar{c})\left((c^2 + q_1)\,KcJ_0(Kc) + qJ_1(Kc)\right)\right\} = 0, \tag{88}$$

where

$$q = q_2 - q_1. \tag{89}$$

By introducing the symbols

$$\mathrm{Ber}_k = \operatorname{Re}\{J_k(Kc)\}; \qquad \mathrm{Bei}_k = \operatorname{Im}\{J_k(Kc)\}, \tag{90}$$

the eigenvalue Eq. (88) can be written in the following form:

$$\begin{aligned} &(d_1\,\mathrm{Ber}_1 + d_2\,\mathrm{Bei}_1)\,(d_4\,\mathrm{Bei}_0 + d_5\,\mathrm{Ber}_0 + q\,\mathrm{Bei}_1) \\ &- (d_1\,\mathrm{Bei}_1 - d_2\,\mathrm{Ber}_1)\,(d_4\,\mathrm{Ber}_0 - d_5\,\mathrm{Bei}_0 + q\,\mathrm{Ber}_1) = 0, \end{aligned} \tag{91}$$

with

$$\begin{aligned} d_1 &= \delta^2 - M^2 + N^2, \qquad d_2 = 2MN, \qquad d_3 = q_1 + M^2 - N^2, \\ d_4 &= K(Md_3 - Nd_2), \qquad d_5 = K(Md_2 + Nd_3). \end{aligned} \tag{92}$$

The above representation (91) of the eigenvalue equation differs from the one presented by Cheng et al. [5], where, as also stated by Hutchinson and Miles [6], some misplacement is contained.

EI-Regime

In *EI* the solution of (78) reads:

$$\hat{u} = C_1 I_1(Kc_1\varrho) + C_2 I_1(Kc_2\varrho), \tag{93}$$

where I_1 is the modified Bessel function of the first order and first kind, and $c_{1/2}$ are given by (55). The eigenvalue equation in *EI* takes the following form:

$$\begin{aligned} &\{Kc_1(c_1^2 - q_1)\, I_0(Kc_1) - qI_1(Kc_1)\}\,(c_2^2 + \delta^2)\, I_1(Kc_2) \\ &- \{Kc_2(c_2^2 - q_1)\, I_0(Kc_2) - qI_1(Kc_2)\}\,(c_1^2 + \delta^2)\, I_1(Kc_1) = 0. \end{aligned} \tag{94}$$

EC/H-Boundary

With c from (59) and $J_k = J_k(Kc)$, the eigenvalue equation on *EC/H* reads:

$$b(KcJ_0)^2 + 2(b_1 - b)\, KcJ_0J_1 + \left(b_2 + b(Kc)^2\right) J_1^2 = 0, \tag{95}$$

with

$$\begin{aligned} b &= (c^2 + q_1)\,(c^2 - \delta^2) \\ b_1 &= c^2(q_1 + \delta^2); \qquad b_2 = 2c^2q. \end{aligned} \tag{96}$$

Short Wave-Length Limit

For $m \to \infty$ ($K \to \infty$) the eigenvalue Eqs. (88) and (94) degenerate to the same equation, thereby characterizing the short wave-length limit in *E*:

$$\left(\frac{1 - \dfrac{t}{\mu}}{1 + \dfrac{t}{\mu}}\right)^{1/2} = \frac{2\lambda\delta\,\dfrac{t}{\mu}}{(2\delta^2 \pm ah_t)\,\dfrac{t}{\mu} + \lambda^2\delta^2\,\dfrac{\dot{\mu}}{\mu}}. \tag{97}$$

From (96) it can be seen that on *EC/H*

$$c^2 = \delta^2 \Leftrightarrow \frac{t}{\mu}\,\xi_{i,\infty} = (\lambda^2 - \delta^2)/(\lambda^2 + \delta^2) \Rightarrow b = 0, \tag{98}$$

and consequently (95) yields

$$J_1(K\delta) = 0, \tag{99}$$

which asymptotically is satisfied by

$$K\delta = (n + 1/4)\,\pi \qquad (n \to \infty). \tag{100}$$

This means that $\xi_{i,\infty}$ is an accumulation point of solutions on *EC/H*, and consequently at this point $K \to \infty$ is also a solution.

Computational Results and Discussion

The main part of the computational effort refers to the evaluation of the eigenvalue equation in the *EC*-regime (91). For the computation of (90), the complex Bessel-functions subroutine by Zimmerman et al. [23] has been used. The results are plotted in (t/μ vs. h_t)-diagrams, where contours of constant maximum critical slenderness (R/H) are depicted.

The eigenvalue Eqs. (91), (94), (95), and (97) are evaluated for some material properties which are characteristic for dense, medium-grained Karlsruhe sand. The corresponding material properties are taken from Goldscheider [16], [24]. The computations showed that the analysis can be restricted in the vicinity of the peak of the assumed stress ratio-strain curves, where the mobilized friction angle is approximately equal to its maximum value ϕ_p. From the Mohr-Coulomb limit condition given in [16] it follows that $\phi_p \simeq 40°$ (initial porosity $n_1 \simeq 0.365$). As mentioned above, the deviatoric flow rule given in [16] can be approximated by $\chi = 0.55$ [11]. The dilatancy characteristics of this sand are taken from [24], and thus the computations are performed with $\beta = 0.3$ ($\phi_c \simeq 30°$).

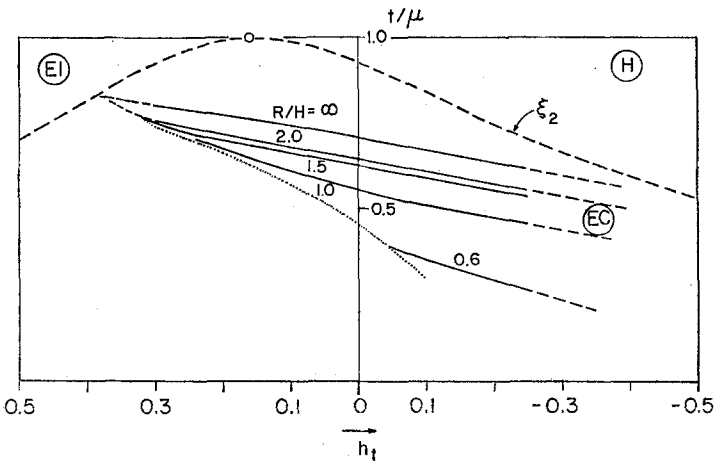

Fig. 6. Diffuse bulging in the triaxial compression test ($m = 1$; $\phi_p = 40°$, $\phi_c = 30°$, $\chi = 0$)

Fig. 6 and 7 show the computational result for triaxial compression and for the 'half-wave length mode' (see Fig. 1b; $m = 1$ in (75)). Fig. 6 corresponds to the von Mises deviatoric flow rule $\chi = 0.$; whereas, Fig. 7 corresponds to the true one for $\chi = 0.55$. By comparing these two Figs., it follows that the deviation from the von Mises deviatoric flow rule is destablizing the system by reducing the critical bifurcation stress $(t/\mu)_{R/H}$, which corresponds to some slenderness (R/H) and hardening rate h_t. Taking into account that diffuse bulging modes are observed experimentally for $R/H = 0.6$ [7], Fig. 6 can be used to show that the deformation theory of plasticity, holding for $\chi = 0.$, cannot predict the experimental findings. From (33) it follows that in this case $(t/\mu) = g$,

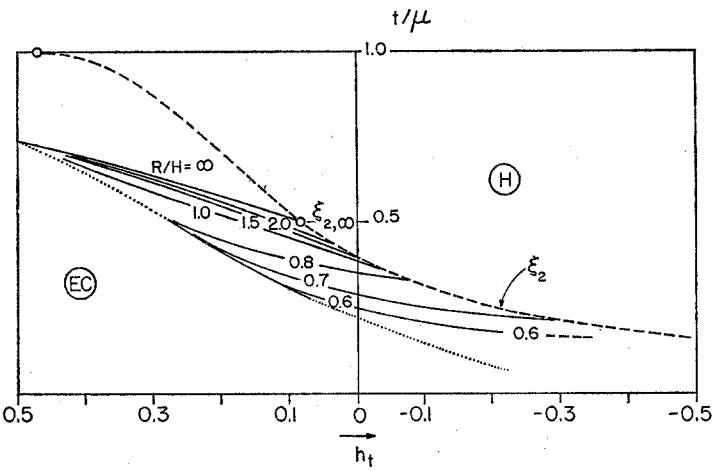

Fig. 7. Diffuse bulging in the triaxial compression test ($m = 1$; $\phi_p = 40°$, $\phi_c = 30°$, $\chi = 0.55$)

and from Fig. 3a and 3b it follows that the shearing strain intensity is at peak $g_p \simeq 0.13$. On the other hand, (35) can yield an expression for h_1:

$$h_1 = \frac{\pm 1}{1 \pm \chi/2} \frac{\sin \phi_a}{(t/\mu)}. \tag{101}$$

From Fig. 7 and for $R/H = 0.6$ an estimate for h_1 at the plastic limiting state ($h_t = 0$) can be derived:

$$h_1 = \frac{1}{1 + 0.55/2} \cdot \frac{0.545}{0.25} = 1.71 < h_s = \frac{0.545}{0.13} = 4.19. \tag{102}$$

At peak the true hardening rate h_1 is about 2.5-times lower than the corresponding secant modulus h_s.

Taking into account that bulging in the compression test is not observed for $R/H = 1.44$ [21], from Fig. 7 it follows that the true (t/μ vs. h_t)-state path will not intersect the $R/H \geqq 1.5$ contours. Consequently, the true state path will intersect the EC/H-boundary in the softening regime ($h_t < 0$); i.e., localizations in the triaxial compression test, with lubricated end platens, will occur in the softening regime. This result is also in accordance with the experimental evidence [7].

Figs. 8 and 9 show the computational results for triaxial extension and for the 'full-wave length mode' (see Fig. 1c; $m = 2$ in (75)), as well as for $\chi = 0.$ and $\chi = 0.55$, respectively. For extension the consideration of the true deviatoric flow rule has a stabilizing effect. With h_1 estimated from (102), the actual value of (t/μ) in the vicinity of the plastic limiting state can be computed by means of (101):

$$t/\mu = \begin{cases} -0.21 & \text{for} \quad \chi = 0. \\ -0.29 & \text{for} \quad \chi = 0.55. \end{cases} \tag{103}$$

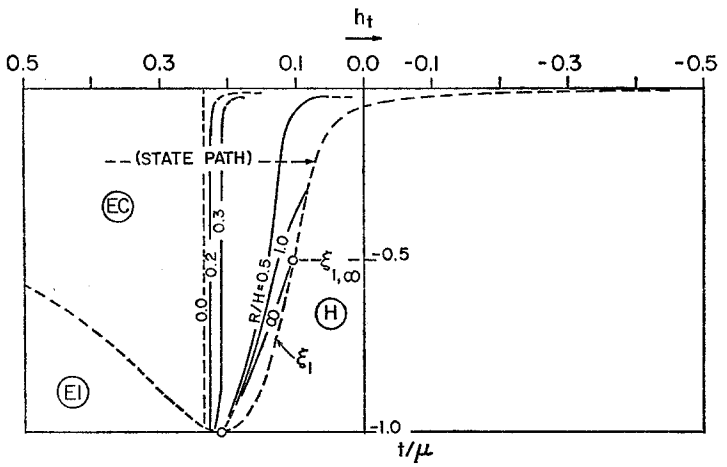

Fig. 8. Diffuse necking in the triaxial extension test
($m = 2$; $\phi_p = 40°$, $\phi_c = 30°$, $\chi = 0$)

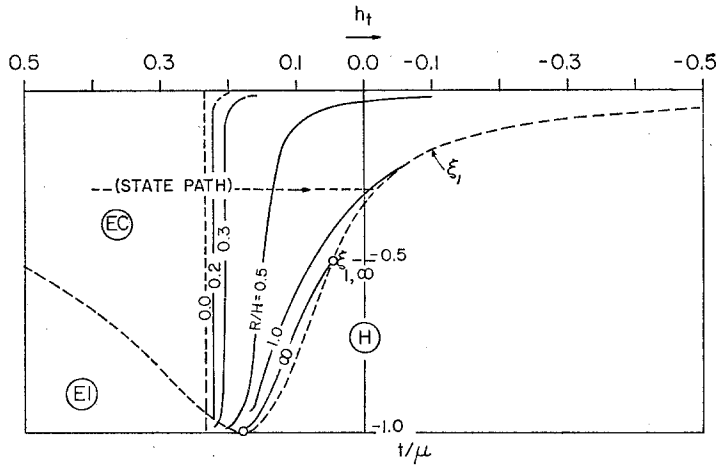

Fig. 9. Diffuse necking in the triaxial extension test
($m = 2$; $\phi_p = 40°$, $\phi_c = 30°$, $\chi = 0.55$)

These values are indicated in Figs. 8 and 9 as the estimated 'state path'. Consequently, diffuse necking will always precede localized necking, the latter always occurring in the vicinity of the peak state of stress.

Fig. 10 shows the computed orientation angle ψ of the localization on EC/H as a function of the hardening rate. As already mentioned, ψ tends for small t/μ-values to the value ψ_B given by (69). Let

$$\psi_C = 45° \pm \phi_p/2 \tag{104}$$

denote the so-called Coulomb value of ψ. The underlying Coulomb failure criterion is that the orientation of the localization coincides with the planes of maximum

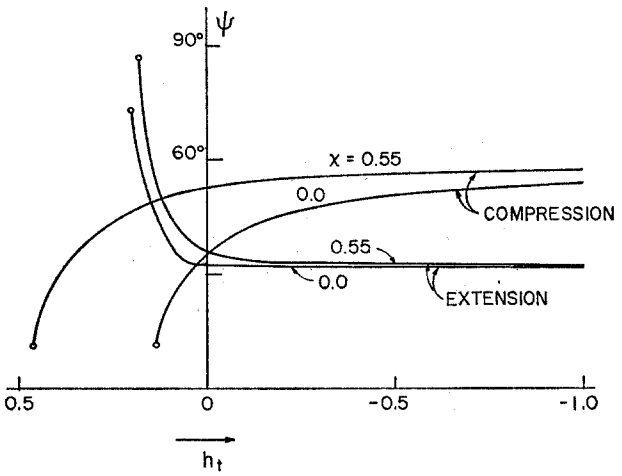

Fig. 10. Orientation angle of the localization in triaxial compression and extension ($\phi_p = 40°$, $\phi_c = 30°$, $\chi = 0.$ and $\chi = 0.55$)

stress obliquity, i.e., of maximum shear stress/normal stress ratio. For the considered computational examples it is:

$$\psi_C = \begin{cases} 65° \\ 25° \end{cases}; \qquad \psi_B = \begin{cases} 58.5° \\ 31.5° \end{cases}, \tag{105}$$

for compression and extension, respectively. From (105) it follows that the Coulomb criterion is not compatible with an exact bifurcation analysis. The same result was also obtained from the bifurcation analysis of plane rectilinear deformations [2], [18]. The present theoretical prediction for $\psi = \psi_B$, can be supported from the experimental evidence. From Bishop and Green [25], Fig. 7a, it follows that a slender lubricated specimen of medium-dense, Ham-River sand has failed along a shear band inclined at an angle $\psi \simeq 58°$. From Figs. 12 and 14 of the same reference, it follows that for the considered sand ($n_1 \simeq 0.414$) $\phi_p \simeq 39°$, $\phi_c \simeq 31°$ ($\delta^2 = 1.41$). Introducing these values into (69) and (104) yields: $\psi_B = 57.6°$, $\psi_C = 64.5°$, which means that the bifurcation analysis produces the correct value for ψ. It should be noted that from the information given in [25], it follows that localization in the considered compression test took place in the softening regime; i.e., the present theory is fully consistent with the experimental evidence.

Acknowledgement

The author wants to thank the Graduate School of the University of Minnesota for supporting the research program of the present study (Grant No. 483-0350-4909-02).

References

[1] Needleman, A.: Non-normality and bifurcation in plane strain tension and compression. J. Mech. Phys. Solids **27**, 231–254 (1979).

[2] Vardoulakis, I.: Bifurcation analysis of the plane rectilinear deformation on dry sand samples. Int. J. Solids Structures **17**, 1085–1101 (1981).

[3] Hill, R., Hutchinson, J. W.: Bifurcation phenomena in the plane tension test. J. Mech. Phys. Solids **23**, 239—264 (1975).
[4] Young, N. J. B.: Bifurcation phenomena in the plane compression test. J. Mech. Phys. Solids **24**, 77—91 (1976).
[5] Cheng, S. Y., Ariaratnam, S. T., Dubey, R. N.: Axisymmetric bifurcation in a elastic-plastic cylinder under axial load and lateral hydrostatic pressure. Quart. Appl. Mathematics **29**, 41—51 (1971).
[6] Hutchinson, J. W., Miles, J. P.: Bifurcation analysis of the onset of necking in an elastic/plastic cylinder under uniaxial tension. J. Mech. Phys. Solids **22**, 61—71 (1974).
[7] Vardoulakis, I.: Bifurcation analysis of the triaxial test on sand samples. Acta Mechanica **32**, 35—54 (1979).
[8] Stören, S., Rice, J. R.: Localized necking in thin sheats. J. Mech. Phys. Solids **23**, 421—441 (1975).
[9] Vardoulakis, I.: Constitutive properties of dry sand, observable in the triaxial test. Acta Mechanica **38**, 219—239 (1981).
[10] Rudnicki, J. W., Rice, J. R.: Conditions for the localization of the deformation in pressure-sensitive dilatant materials. J. Mech. Phys. Solids **23**, 371—394 (1975).
[11] Vardoulakis, I.: Rigid granular model for sand and the influence of the deviatoric flow rule. Mech. Res. Comm. **8**, 275—280 (1981).
[12] Shanley, F. R.: Inelastic column theory. I. Aeronaut. Sci. **14**, 261—268 (1947).
[13] Thomas, T. Y.: Plastic flow and fracture in solids. New York: Academic Press 1961.
[14] Truesdell, C., Noll, W.: Non-linear field theories of mechanics. (Flügge's Handbuch der Physik, III/3.) Berlin—Heidelberg—New York: Springer 1965.
[15] Vardoulakis, I.: Equilibrium bifurcation of granular earth bodies. Advances in Analysis of Geotechnical Instabilities, University of Waterloo Press, SM Study No. 13, 65—119 (1978).
[16] Goldscheider, M.: Grenzbedingung und Fließregel von Sand. Mech. Res. Comm. **3**, 463—468 (1976).
[17] Kolymbas, D.: A rate-dependent constitutive equation for soils. Mech. Res. Comm. **4**, 367—372 (1977).
[18] Vardoulakis, I.: Shear band inclination and shear modulus of sand in biaxial tests. Int. J. Num. Anal. Meth. Geomech. **4**, 103—119 (1980).
[19] Mehrabadi, M. M., Cowin, S. C.: Prefailure and post-failure soil plasticity models. ASCE J. Engr. Mech. Div. Proc. **106**, 991—1003 (1980).
[20] Rowe, P. W.: Theoretical meaning and observed values of deformation parameters for soil. Proc. Roscoe Mem. Symp., Cambridge University (Perry, R. H. G., ed.), pp. 143—194. 1971.
[21] Hettler, A.: Verschiebungen starrer und elastischer Gründungskörper in Sand bei monotoner und zyklischer Belastung. Dissertation, Universität Karlsruhe, 1981.
[22] Reads, D. W., Green, G. E.: Independent stress control and triaxial extension tests on sand. Geotechnique **26**, 551—576 (1976).
[23] Zimmerman, K. L., Elder, A. S., Depue, A. K.: Users manual for the BRL subroutine to calculate Bessel functions of integral order and complex argument. Tech. Report ARBRL-TR-02068, U.S. Army Armament Res. and Dev. Cmd., Ballistic Res. Lab., Aberdeen (1978).
[24] Goldscheider, M.: Materialverhalten von Sand. Manuscript. Oberwolfach Jan. 1977.
[25] Bishop, A. W., Green, G. E.: The influence of end restraint on the compression strength of cohensionless soil. Geotechnique **23**, 243—266 (1973).

Prof. Dr. I. Vardoulakis
Department of Civil and Mineral Engineering
University of Minnesota
Minneapolis, MN 55455, U.S.A.